Possible interaction mechanism for quaternary ammonium (QA) ions binding to potassium channels: density functional theory and MP2 studies on the interaction between phenol and ammonium cation †

Xiao Jian Tan, Hua Liang Jiang,* Wei Liang Zhu, Kai Xian Chen * and Ru Yun Ji

Shanghai Institute of Materia Medica, Chinese Academy of Sciences, Shanghai 200031, China. E-mail: jiang@iris3.simm.ac.cn

Received (in Cambridge) 31st July 1998, Accepted 4th November 1998

Tetraethylammonium (TEA) and other quaternary ammonium (QA) ions are potent blockers of potassium channels. In order to shed light on the blockade mechanism of QA ions, we have carried out a series of computations on the phenol–ammonium model with density functional theory (DFT) and Möller–Plesset second order perturbation (MP2) methods at levels of 6-31G* and 6-31G** basis sets. NH–aromatic π interaction and NH–OH hydrogen bond interaction, which are important in biological systems, are responsible for the binding of NH_4^+ to phenol. From analysis of structures, energies, charge populations and transition state features, both the cation–π interaction and hydrogen bond or electrostatic interaction between QAs and the key amino acid residues at the entryways of K^+ channels are seen to be significant in the blockade mechanism of QA ions.

Introduction

Tetraethylammonium (TEA) ion and other quaternary ammonium (QA) ions can inhibit potassium channels by binding within the ion conduction pore.[1–4] Most K^+ channels are inhibited by QA ions applied to either the intracellular or extracellular entryway. Several experimental findings[1–3,5] and the X-ray crystal structure of the K^+ channel from *Streptomyces lividans* (KcsA K^+ channel) released recently by Doyle *et al.*[6] support this conclusion. Mutation studies have shown that one specific amino acid location in the external mouth of the entryway (position 449 of the *Shaker* K^+ channel and position 82 of the KcsA K^+ channel) is critical in determining sensitivity to external TEA.[6–9] Two electrode voltage clamp measurements have shown that the TEA affinities with different amino acids substituted at position 449 of the *Shaker* K^+ channel have a sequence of phenylalanine (F) > tyrosine (Y) > tryptophan (W) > threonine (T) ≈ serine (S) > isoleucine (I) > valine (V),[9] from which we can see that TEA affinities with the aromatic residue and hydroxy-containing residue mutated channels are higher than those of the hydrophobic residue substituted channels. In addition, MacKinnon *et al.*[9] found the temperature dependence of the blockade, suggesting that TEA affinity to the *Shaker* K^+ channel was not a pure hydrophobic effect. Based on these findings, the cation–π interaction was thought to have a part in the blocking mechanism by which QA ions inhibit K^+ channels.[9,10] However, the TEA affinity of the K^+ channels whose entryways are composed of serines or threonines, such as wide type *Shaker*, *clost*, *parame* and *celegans* K^+ channels, cannot be rationalised by cation–π interaction, although, threonine is a key residue for TEA binding from the intracellular solution.[7] Structurally, serine and threonine share a common feature at their side chains, *i.e.* both residues contain a hydroxy group at the β carbon. Does this hydroxy play an important role in the TEA blockade? So far, no report has been seen to answer this question.

In order to interpret the experimental results and clarify the mechanism of the association between QA ions and potassium channels, we have performed a theoretical study choosing phenol–ammonium complex as a model molecule employing density functional theory (DFT) and Möller–Plesset second order perturbation (MP2) approaches at basis set levels of 6-31G* and 6-31G**, respectively. Though phenol–ammonium interaction has been investigated by Basch *et al.*,[11] their study focused on the cation–π interaction. Differing from theirs, our study involved a series of computations on the interaction of phenol and ammonium in the gas phase, especially the transition state, and different interaction models were addressed according to our calculations. In addition, we have used more sophisticated theoretical methods in our calculations, namely DFT and MP2, and larger basis sets, 6-31G* and 6-31G**, than those of the Basch group, which used only an MP2/6-31G*//3-21G approach.

Our computation gave two kinds of stable structures of phenol–ammonium complex corresponding to two different mechanisms. The phenol–ammonium complex of the *en face* mechanism adopts the structure such that two N–H bonds of NH_4^+ are directed towards the benzene ring through cation–π interaction, and the complex of the oxygen cage mechanism has the structure in which one N–H hydrogen bonds to the oxygen of hydroxy. The second complex is about 4.25 kcal mol^{-1} more stable than the first complex. Finally, the structure of the transition state was obtained, and the energy calculations indicate that there is almost no barrier between the first and the second complexes. More importantly, new results are obtained leading to a suggestion for a possible mechanism of QA ions bonding to potassium channels.

Computational details

The geometries of the models

For the phenol–ammonium complex of the oxygen cage mechanism, three initial geometries were selected during the calculation, *i.e.* the structures with one N–H bond, two N–H bonds and three N–H bonds directed toward the oxygen atom of hydroxy, respectively (Fig. 1, **1a**–**1c**). For the phenol–ammonium complex of the *en face* mechanism, we also

† This project was supported by Grant 29725203 from the National Natural Science Foundation of China, and Grant 863-103-04-01 from the "863" High Technology Program of China.

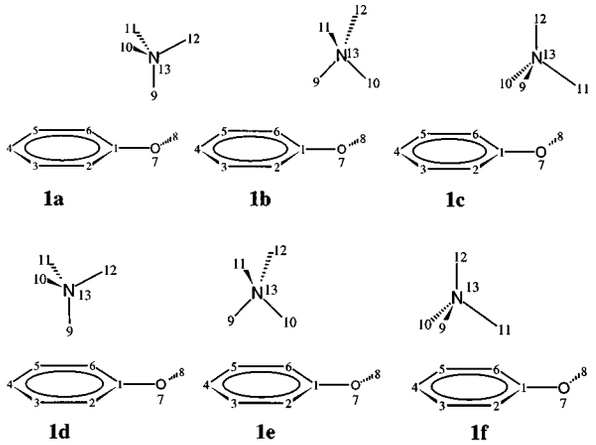

Fig. 1 The possible initial geometries of the phenol–ammonium complex.

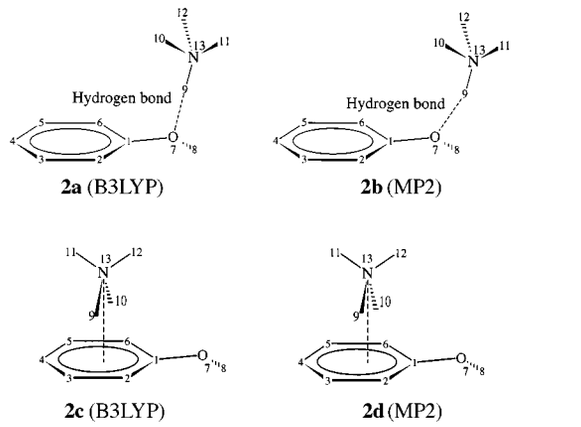

Fig. 2 The optimized geometries with B3LYP/6-31G* and MP2/6-31G** for oxygen cage complexes (**2a**, **2b**) and *en face* complexes (**2c**, **2d**).

considered three initial conformers according to the number of the N–H bonds directed toward the benzene ring (Fig. 1, **1d**–**1f**).

Computational methods

The calculations were performed in two steps. First, an optimization of the geometry was carried out by using B3LYP, a density functional theory (DFT) type of calculation based on hybrid functionals.[12] Frequency calculation was then carried out for each optimized structure to see whether they were real minimum energy structures in the potential surface. In the second step, the most stable structures of the two complexes derived by the B3LYP method were reoptimized with the MP2 approach at the level of the 6-31G** basis set, and frequency calculation was then performed using MP2/6-31G** to verify the reasonability of the results of the B3LYP/6-31G* method.

In order to demonstrate the kinetic features between the two complexes, the structure of the transition state between the two complexes was searched with the B3LYP/6-31G* approach and then the MP2/6-31G** method. Frequency calculations were also carried out for the optimized transition states with the above two quantum chemical methods, and vibration analysis for the negative frequency was performed to test and verify the structure of the transition state.

Results and discussion

The geometries of the complexes

B3LYP/6-31G* optimized results indicated that all the initial geometries of the oxygen cage mechanism complexes converged into the structure that has one N–H bond oriented to the oxygen atom of the hydroxy. Further analysis suggested that a hydrogen bond and electrostatic binding formed between ammonium and phenol (Fig. 2, geometry **2a**). Frequency calculation on the optimized structure with the B3LYP/6-31G* method showed that no negative frequency exists, indicating the final optimized structure was the minimum energy structure. Based on the B3LYP/6-31G* result, the geometry of the oxygen cage complex was reoptimized with the more sophisticated method MP2/6-31G**, and then frequency calculation was performed on the MP2 optimized structure with the same method. There is no negative frequency in the MP2 optimized structure, which indicated that a real energy minimum structure was addressed by MP2/6-31G**. The geometry of MP2/6-31G** (Fig. 2, geometry **2b**) is very similar to that of B3LYP/6-31G*. Using the same calculation strategy, the three initial structures of cation–π complexes were optimized by B3LYP/6-31G* and MP2/6-31G**. Geometries **1d** and **1f** were converged into the structure with two N–H bonds directed toward the benzene ring (Fig. 2, geometries **2c** and **2d**), while geometry **1e** was converted into the stable configuration of an oxygen cage complex. The structural parameters of each stable configuration are listed in Table 1.

Comparing the bond lengths of the two complexes with those of the monomeric states of phenol and ammonium, some interesting phenomena can be noted. In the oxygen cage complex, the C–C bond lengths were shortened because of the NH_4^+ interaction (Table 1). The reason for this phenomenon might be that the interaction of NH_4^+ with the lone pair electrons of hydroxy may reduce the conjugate effect between hydroxy and benzene, which 'locks' the π electrons in the benzene. The reduction of the conjugate effect between hydroxy and the benzene ring in the oxygen cage complex can be seen from the C–O bond length, which is 0.05 Å longer than that of phenol (Table 1). While in the *en face* complex, the C–C bond lengths are about 0.006 Å longer than those of phenol, indicating π electrons in the benzene ring have been partially transferred to NH_4^+ through cation–π interaction (see the following discussion of charge). This reduces the π electron cloud of the benzene ring, which decreases π–bond interaction among the carbon atoms, and thereby the C–C bonds are lengthened. Of particular interest is that the C–O bond length of the *en face* complex is about 0.01 Å shorter than that of phenol (Table 1). We deduce that the induction effect of NH_4^+ increases the conjugation of lone-pair electrons of the hydroxy oxygen with the benzene ring, which shortens the C–O bond length.

From the above discussion, we can conclude that electron transfer might occur between the hydroxy oxygen and NH_4^+ for the oxygen cage complex, and between the benzene ring and NH_4^+ for the *en face* complex. This will be further demonstrated in the following section.

Charge population analysis

Tables 2 and 3 respectively present the atomic charges and group charges of each complex. The group charge was calculated by the summation over all the atomic charges of the atoms that compose the group. In general, the charge of NH_4^+ reduced and that of the phenol increased in the two complexes (Table 3), indicating that electron transfer from phenol to NH_4^+ had occurred. However, the electron transfer mechanism is different for these two complex models. For the *en face* complex, the electron transfer is mainly from benzene to NH_4^+, and this electron transfer drives the lone pair electrons of hydroxy oxygen to move to the benzene ring (Table 2), which enhances the conjugation between hydroxy and the benzene ring. This can be seen from the C–O bond length (Table 1), which in the *en face* complex is shorter than that in phenol. For the oxygen cage complex, because of the induction effect of NH_4^+, the lone pair electrons cannot conjugate with the benzene ring, which makes

Table 1 Some important bond lengths (Å) and angles (°) for each molecule (the atomic numbering used is shown in Fig. 2)

	Oxygen model		*en face* model		Single molecule	
Atom No.	B3LYP	MP2	B3LYP	MP2	B3LYP	MP2
1–2	1.392	1.393	1.408	1.405	1.399	1.397
2–3	1.397	1.397	1.400	1.396	1.393	1.393
3–4	1.396	1.396	1.402	1.402	1.398	1.398
4–5	1.396	1.396	1.399	1.401	1.395	1.395
5–6	1.397	1.396	1.402	1.400	1.396	1.396
6–1	1.392	1.392	1.405	1.402	1.399	1.397
1–7	1.411	1.410	1.355	1.361	1.369	1.374
7–8	0.972	0.969	0.972	0.967	0.970	0.965
9–7	1.609	1.620				
9–2			2.289	2.283		
9–3	2.496	2.417	2.370	2.263		
10–4			2.847	2.854		
10–5			2.534	2.532		
9–13	1.077	1.062	1.042	1.035	1.029	1.023
10–13	1.026	1.021	1.033	1.024	1.029	1.023
11–13	1.026	1.019	1.026	1.020	1.029	1.023
12–13	1.026	1.019	1.026	1.020	1.029	1.023
7–13	2.673	2.654	4.041	4.072		
13–ring[a]	4.369	4.093	2.939	2.901		
N–H–O	168.6	163.1				

[a] Represents the distance between the nitrogen and the center of the benzene ring.

Table 2 The atomic charge (Q/e) for each molecule (the atomic numbering used is shown in Fig. 2, 14–18 are the hydrogen atoms attached to carbons 2–6, respectively)

	Oxygen model		*en face* model		Single molecule	
Atom No.	B3LYP	MP2	B3LYP	MP2	B3LYP	MP2
1	0.3092	0.3232	0.3670	0.3982	0.3501	0.3873
2	−0.1872	−0.2284	−0.2316	−0.2590	−0.1584	−0.1814
3	−0.1309	−0.1269	−0.1635	−0.1248	−0.1342	−0.1309
4	−0.1186	−0.1563	−0.1570	−0.2497	−0.1353	−0.1752
5	−0.1330	−0.1281	−0.1666	−0.2557	−0.1332	−0.1299
6	−0.1703	−0.1919	−0.2394	−0.2551	−0.1946	−0.2182
7	−0.7060	−0.7425	−0.6116	−0.6420	−0.6426	−0.6663
8	0.4454	0.3940	0.4318	0.3754	0.4064	0.3526
9	0.4674	0.4723	0.4200	0.3977	0.4609	0.4168
10	0.4326	0.3910	0.4265	0.3886	0.4609	0.4168
11	0.4309	0.3891	0.4365	0.3937	0.4609	0.4168
12	0.4332	0.3906	0.4366	0.3939	0.4609	0.4168
13	−0.8908	−0.7212	−0.8593	−0.6770	−0.8436	−0.6671
14	0.1449	0.1775	0.1931	0.2166	0.1387	0.1666
15	0.1706	0.1910	0.1845	0.2030	0.1307	0.1539
16	0.1725	0.1921	0.1793	0.2006	0.1258	0.1476
17	0.1753	0.1958	0.1840	0.2047	0.1300	0.1535
18	0.1537	0.1787	0.1700	0.1907	0.1165	0.1403

the oxygen more negative than it is in phenol (Table 2). Accordingly, it is not surprising that the benzene ring has a greater positive charge in the oxygen cage complex than in the *en face* complex. As has been discussed above, the conjugation reduction in the oxygen cage complex can also be seen from the C–O bond length, which is longer than that in phenol. Therefore, we can conclude that the electron transfer is from hydroxy to NH_4^+ in the oxygen cage complex.

$$NH_4^+ + C_6H_5OH \longrightarrow NH_4^+ \cdots C_6H_5OH \text{ (complex)}$$

$$\Delta E_{inter} = E_{inter}(\text{complex}) - E_{inter}(NH_4^+) - E_{inter}(C_6H_5OH) \quad (1)$$

$$\Delta E_{therm} = E_{therm}(\text{complex}) - E_{therm}(NH_4^+) - E_{therm}(C_6H_5OH) \quad (2)$$

$$\Delta S = S(\text{complex}) - S(NH_4^+) - S(C_6H_5OH) \quad (3)$$

$$\Delta H = \Delta E_{inter} + \Delta E_{therm} + \Delta(pv) \quad (4)$$

$$\Delta G = \Delta H - T\Delta S \quad (5)$$

The relative stability and binding energies of the two model complexes

Table 4 presents the theoretical results of internal energies (E_{inter}), thermal energies (E_{therm}) and entropies (S) of the two model complexes, NH_4^+ and phenol calculated by B3LYP/6-31G* and MP2/6-31G** methods. The thermodynamic parameters of internal energy change (ΔE_{inter}), thermal energy change (ΔE_{therm}), entropy change (ΔS), enthalpy change (ΔH), and free energy change (ΔG) for the formation of each model complex were calculated using eqns. (1)–(5), and are listed in Table 4. For cation–π systems, the basis set superposition errors (BSSEs) were found to be small.[10,13] On the other hand, our experience on calculating the binding energy of NH_4^+ to benzene indicated that both the B3LYP/6-31G* result and the MP/6-31G* result were perfectly in accordance with experimental data.[14] Therefore, BSSEs were not considered in our theoretical calculations for binding energies. For the two model complexes, as can be seen from Table 4, the oxygen cage model is 4.246 kcal mol^{-1} (DFT result) and 3.826 kcal mol^{-1} (MP2 result) more stable than the *en face* model. This indicates that the hydrogen bonding interaction between NH_4^+ and hydroxy

Table 3 The charges (Q/e) for groups of each molecule

	Oxygen model		*en face* model		Single molecule	
Group	B3LYP	MP2	B3LYP	MP2	B3LYP	MP2
NH_4^+	0.8733	0.7212	0.8603	0.8969	1.0000	1.0000
OH	−0.2595	−0.3485	−0.1798	−0.2666	−0.2362	−0.3137
C_6H_5	0.3862	0.6273	0.3195	0.3697	0.2362	0.3137

Table 4 The calculated energy parameters (E_{inter}: internal energy; E_{therm}: thermal energy; S: entropy; ΔE_{inter}: internal energy change; ΔH: enthalpy change; ΔG: free energy change)

Geometries	Method	E_{inter}/a.u.	E_{therm}/kcal mol^{-1}	S/cal mol^{-1} K	ΔE_{inter}/kcal mol^{-1}	ΔH/kcal mol^{-1}	ΔG/kcal mol^{-1}
Oxygen cage model	B3LYP/6-31G*	−364.394630	103.661	95.063	−22.510	−21.729	−13.796
	MP2/6-31G**	−363.312602	104.943	94.604	−23.120	−22.339	−13.324
Transition state	B3LYP/6-31G*	−364.387070	103.080	90.508	−17.766	−17.566	−8.264
	MP2/6-31G**	−363.305970	104.585	90.691	−18.959	−18.336	−8.155
en face model	B3LYP/6-31G*	−364.388321	103.948	93.785	−18.551	−17.483	−9.158
	MP2/6-31G**	−363.307087	105.111	95.828	−19.660	−18.513	−9.863
NH_4^+	B3LYP/6-31G*	−56.893889	33.077	47.186			
	MP2/6-31G**	−56.733680	33.724	49.329			
C_6H_5OH	B3LYP/6-31G*	−307.464868	69.213	74.538			
	MP2/6-31G**	−306.542076	69.650	75.525			

of phenol is stronger than the cation–π interaction between NH_4^+ and the benzene ring. This also can be seen from the binding thermodynamic parameters of NH_4^+ with phenol (Table 4). For the oxygen cage model, the binding energy, binding enthalpy and binding free energy that derived from the B3LYP/6-31G* result are −22.51, −21.729 and −13.796 kcal mol^{-1}, respectively, and those derived from MP2/6-31G** are −23.12, −22.339 and −13.324 kcal mol^{-1}, respectively. For the *en face* model, the above three values are −18.551, −17.483 and −9.158 kcal mol^{-1} for the B3LYP/6-31G*//6-31G* result, and those for the MP2/6-31G**//6-31G** result are respectively −19.660, −18.513 and −9.863 kcal mol^{-1}. This indicates that NH_4^+ binds to phenol through a hydrogen bond between NH_4^+ and the phenol hydroxy that is about 4 kcal mol^{-1} stronger than the cation–π interaction.

Transition state between the two model complexes

It can be seen from the results of calculating binding thermodynamic parameters for the two models of NH_4^+ to phenol complexation that both complex configurations can naturally exist. To see whether the *en face* complex can change to the oxygen cage complex, a transition state between these two complexes has been searched with both B3LYP/6-31G* and MP2/6-31G** methods.

The structures of transition states optimized by B3LYP/6-31G* and MP2/6-31G** are shown in Fig. 3. To verify the reasonability of the transition states, frequency calculations were performed for both the transition states obtained from the above two theoretical approaches. Each of the transition states has only one imaginary frequency, indicating that these two transition states are located at the saddle points on the reaction potential energy surface.

In order to verify further whether the transition states obtained from B3LYP and MP2 methods are reasonable, vibration normal mode analyses were performed for imaginary frequencies of these two transition states. The vibration modes of the imaginary frequencies are shown in Fig. 3 (represented by arrows). For the two transition states of B3LYP and MP2, the vibration normal modes are the same, which indicated that the B3LYP/6-31G* and MP2/6-31G** results can be in agreement with each other. The geometric parameters (not presented in this paper) of these two transition states also demonstrated this. The imaginary frequency of the transition state is mainly responsible for the stretching vibrations of bonds N13–H9 and N13–H11 toward the benzene ring and the stretching vibration of bond N13–H10 towards the oxygen atom of the hydroxy

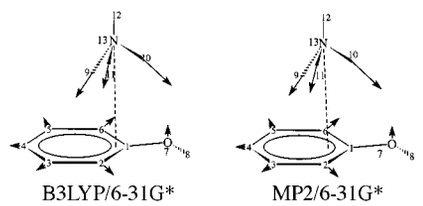

Fig. 3 The normal mode of the imaginary frequency of transition states.

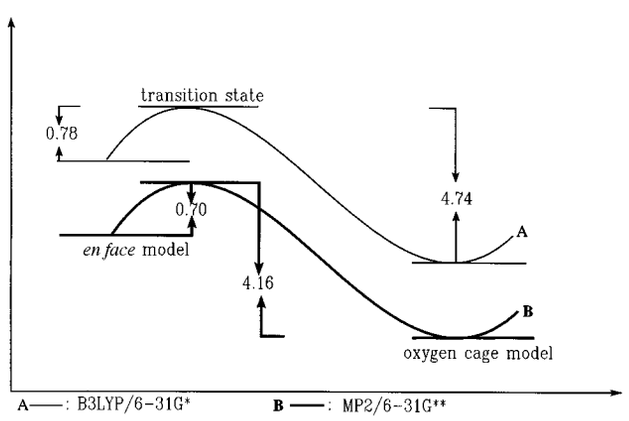

Fig. 4 Schematic representation of the energy profile of the *en face* complex switching to the oxygen cage complex.

group, which reflects the corresponding micro-process of the *en face* complex changing to the oxygen cage complex. This implies that at the transition state, the cation–π interaction between NH_4^+ and the benzene ring is reducing, and the hydrogen bond between NH_4^+ and the oxygen atom of phenol is forming. Accordingly, the structures of the transition states searched by B3LYP/6-31G* and MP2/6-31G** are reasonable.

The energy profile of the *en face* complex converting to the oxygen cage complex is schematically presented in Fig. 4. The calculated energies show barriers for this conversion from both directions (Fig. 4) . The energy barrier for the direction from *en face* complex to oxygen cage complex is surprisingly low, 0.78 kcal mol^{-1} for the B3LYP/6-31G* result and 0.70 kcal mol^{-1} for the MP2/6-31G** result. From Table 4, we can also calculate the activation enthalpy and activation free energy. For the direction from *en face* complex to oxygen cage, the activation enthalpies are −0.083 kcal mol^{-1} for the B3LYP result and 0.177 kcal mol^{-1} for the MP2 result, and the activation free

energies for the two theoretical results are respectively 0.894 and 1.708 kcal mol^{-1}. Therefore, it is very easy for the *en face* complex to change to the oxygen cage complex, and the total conversion is exothermic, the reaction enthalpy and free energy being about 4.246 and 4.638 kcal mol^{-1} (DFT result), respectively. According to the above discussion we can conclude that the final configuration of NH_4^+ binding to phenol is the oxygen cage complex.

Possible interaction mechanism for QA ions binding to potassium channels

Most K^+ channels are inhibited by QA ions applied to either the intracellular or extracellular surface. They appear to be located very near the pore opening on either side of the membrane.[9] Recently, the X-ray crystal structure of the K^+ channel from *Streptomyces lividans* (KcsA K^+ channel) has been determined by Doyle *et al*,[6] indicating that the mouth of the extracellular entryway is composed of four tyrosines (Tyr82 for KcsA K^+ channel) with the hydroxy groups facing to the outside of the cell, and the intracellular entryway is compiled of several aromatic amino acids. According to this and our calculation result, we can explain some of the blockade mechanisms of QA ions inhibiting K^+ channels.

As has been revealed above, NH_4^+ can bind with phenol through both a hydrogen bond between NH_4^+ and the hydroxy group and cation–π interaction, and the hydrogen bond interaction is the stronger of the two. This indicates that either of these two interactions is essential for QA ions blocking K^+ channels.

For the blocking mechanism of QA ions at the inner mouth of K^+ channels, there is an argument that cation–π interaction is the driving force for QA ions binding to K^+ channels. Our calculation and others' calculations[10] are in line with this deduction. However, for the blockade of QA ions at the outer mouth of K^+ channels, the importance of the hydrogen bond or electrostatic interaction between QA ions and the hydroxy of tyrosine (take KcsA K^+ channel as an example) has not been appreciated so far. From our calculation results of the NH_4^+–C_6H_5OH model system, the binding energy of oxygen cage complex formation is greater than that of cation–π interaction (Table 4). Accordingly, we deduce that the binding strength between other QA ions and the hydroxy group at least can compete with the cation–π interaction. The energy barrier between the oxygen cage complex and the *en face* complex is not too high, just about 4.7 kcal mol^{-1} (Fig. 4). For other QA ions, it might be lower than this value due to the weaker interaction between QA ions and the hydroxy group. So it is easy for the oxygen cage complex to switch to the *en face* complex. We therefore conclude that with respect to the QA ions blocking K^+ channels at the outside receptor site, the hydrogen binding or electrostatic interaction between QA ions and especially hydroxy at the outside mouth can be the first driving force. The wide type *Shaker* K^+ channel is blocked at the outside mouth by TEA.[9] Interestingly, there is no aromatic amino acid at position 449 of the wide type *Shaker* K^+ channel (corresponding to tyrosine 82 of KcsA K^+ channel). However, there is a threonine at this position. It is very clear that a hydroxy group attaches to threonine, which can interact with TEA through a hydrogen bond or electrostatics.

The mutation experiment suggested that serine substituted *Shaker* K^+ channel at position 449 had the same TEA affinity as the wide type K^+ channel.[9] According to our calculation result, it is not surprising that serine substitution did not change the TEA binding affinity because either threonine or serine has a hydroxy at the β carbon atom. There are other types of K^+ channels, such as *clost*, *parame*, *celegans*, and the lips of their extracellular entryways are composed of four serines or four threonines. For these K^+ channels, cation–π interaction cannot explain the TEA affinity, but our calculations can.

Based on the calculation results in this paper and the mutation experiments,[9,15] we propose an affinity mechanism for QA ions blocking K^+ channels: (1) For the K^+ channel that has tyrosines at the extracellular entryway, such as KcsA K^+ channel, both hydrogen bond or electrostatic interaction and cation–π interaction between QA ions and tyrosines are important for QA affinity. According to the X-ray structure of KcsA K^+ channel,[6] we deduce that the hydrogen bond or electrostatic interaction is the first driving force for QA ions affinity, and the QA–channel complex converts to an *en face* complex through cation–π interaction. (2) For the K^+ channel that has serine or threonine at the extracellular entryway, such as the wide type *Shaker* K^+ channel, QA ions affinity comes only from hydrogen bond or electrostatic interaction between QA and the hydroxy group of serine or threonine. (3) Comparing the structures of serine and threonine with that of tyronine, we can see that one of the reasons why TEA affinity of serine substituted or threonine substituted *Shaker* K^+ channel[9,15] is weaker than that of tyrosine substituted *Shaker* K^+ channel is that the side chain of serine or threonine is shorter than that of tyrosine, which means that QA ions like TEA cannot interact with the four hydroxys in serines or threonine simultaneously. To mimic the structure of tyrosine, we predict that if someone can extend the side chain of serine or threonine to a structure such as **1**, and use this abnormal amino acid as a substitute for serine at position 449 of *Shaker* K^+ channel the TEA affinity will be increased and may be compared with tyrosine substituted *Shaker* K^+ channel.

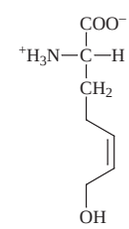

1

Acknowledgements

The authors are grateful to The Network Information Center, Chinese Academy of Sciences for offering us computational facilities. We gratefully acknowledge financial support from National Natural Science Foundation of China (Grant 29725203) and "863" High Technology program of China (Grant 863-103-04-01).

References

1 B. Hill, *J. Gen. Physiol.*, 1967, **50**, 1287.
2 C. M. Armstrong, *J. Gen. Physiol.*, 1971, **58**, 413.
3 R. J. French and R. J. Shoukimas, *Biophys. J.*, 1981, **34**, 271.
4 R. J. French and R. J. Shoukimas, *Biophys. J.*, 1981, **34**, 271.
5 G. Yellen, M. T. Abramson and R. MacKinnon, *Science*, 1991, **251**, 939.
6 D. A. Doyle, J. M. Cabral, R. A. Pfuetzner, A. Kuo, J. M. Gulbis, S. L. Cohen, B. T. Chait and R. MacKinnon, *Science*, 1998, **280**, 69.
7 R. MacKinnon and G. Yellen, *Science*, 1990, **250**, 276.
8 M. P. Kavanaugh, M. D. Varnum, P. B. Osborne, M. J. Christie, A. E. Busch, J. P. Adelman and R. A. North, *J. Biol. Chem.*, 1991, **266**, 7583.
9 L. Heginbotham and R. MacKinnon, *Neuron*, 1992, **8**, 483.
10 J. C. Ma and D. A. Dougherty, *Chem. Rev.*, 1997, **97**, 1303.
11 H. Basch and W. J. Stevens, *J. Mol. Struct.* (*THEOCHEM*), 1995, **338**, 303.
12 A. D. Becke, *J. Chem. Phys.*, 1993, **93**, 5648.
13 S. Mecozzi, A. P. West, Jr. and D. A. Dougherty, *Proc. Natl. Acad. Sci.*, 1996, **93**, 10566.
14 Hua Liang Jiang, Wei Liang Zhu, Xiao Jian Tan, Jian De Gu, Jian Zhong Chen, Mao Wei Lin, Kai Xian Chen and Ru Yun Ji, *Sci. China*, *Ser. B*, 1998, **41**, 535.
15 L. Choi, C. Mossman, J. Aube and G. Yellen, *Neuron*, 1993, **10**, 533.

Paper 8/06009F